

Flexible LED Index Modulation for MIMO Optical Wireless Communications

Anil Yesilkaya*, Ardimas Andi Purwita*, Erdal Panayirci[†], H. Vincent Poor[‡] and Harald Haas*

*Institute for Digital Communications, LiFi R&D Centre, The University of Edinburgh, Edinburgh EH9 3JL, UK

Email: {a.yesilkaya, a.purwita, h.haas}@ed.ac.uk

[†]Department of Electrical and Electronics Engineering, Kadir Has University, 34083, Istanbul, Turkey

Email: eepanay@khas.edu.tr

[‡]Department of Electrical Engineering, Princeton University, NJ-08544, USA

Email: poor@princeton.edu

Abstract—The limited bandwidth of optical wireless communication (OWC) front-end devices motivates the use of multiple-input-multiple-output (MIMO) techniques to enhance data rates. It is known that very high multiplexing gains can be achieved by spatial multiplexing (SMX) at the cost of prohibitive detection complexity. Alternatively, in spatial modulation (SM), a single light emitting diode (LED) is activated per time instance where information is carried by both the signal and the LED index. Since only one LED is active, both the transmitter (TX) and receiver (RX) complexity reduce significantly while retaining the information transmission in the spatial domain. However, this simplified TX utilization approach leads SM to suffer from significant spectral efficiency losses compared to SMX. In this paper, we propose a technique that benefits from the advantages of both systems. Accordingly, the proposed flexible LED index modulation (FLIM) technique harnesses the inactive state of the LEDs as a transmit symbol. Therefore, the number of active LEDs changes in each transmission, unlike conventional techniques. Moreover, the system complexity is reduced by employing a linear minimum mean squared error (MMSE) equalizer and an angle perturbed receiver. Numerical results show that FLIM outperforms the reference systems by at least 6 dB in the low and medium/high spectral efficiency regions.

Index Terms—Optical wireless communications (OWC), multiple-input-multiple-output (MIMO), spatial modulation (SM), minimum mean square equalizer (MMSE).

I. INTRODUCTION

Spatial modulation (SM) is a multiple-input-multiple-output (MIMO) transmission technique which avoids inter-channel interference (ICI) and achieves better power efficiency and error performance [1]. In conventional SM, all but one of the transmitter (TX) units are silenced at a given transmit symbol. Hence, the ICI is completely avoided while sending information by both the transmitted signal (*constellation symbols*) and the

active TX index (*spatial symbols*) simultaneously. Moreover, the detection complexity at the receiver (RX) is significantly reduced in SM as each symbol is transmitted by a single transmit unit. The complexity of SM could be further decreased by omitting the constellation symbols, which leads to space shift keying (SSK) [2]. In SSK, the detection complexity at the RX is simplified in exchange for reduced spectral efficiency. In [3], it is reported that the error performance of SM and SSK are almost equal, which makes SSK a good candidate for low/medium data rate applications. In order to increase the spectral efficiency of SSK, generalized space shift keying (GSSK) is proposed in [4] where multiple TXs are activated per transmission instance. Similarly, generalization of SM, having multiple active transmit units is also proposed in [5] and [6] independently. Note that in generalized spatial modulation (GSM), all the active TXs send the same signal which avoids ICI. The spectral efficiency of GSM is further enhanced by choosing different constellation symbols for each active TX in [7], [8]. Two independent proposals of this idea, namely GSM with multiple active antennas in [7] and multi-stream SM in [8], are referred to as GSM-II throughout this paper. Also, the spectral efficiency of GSSK is improved in optical communications for a 2×2 system in [9]¹. Accordingly, an orthogonal transmission symbol set is proposed to increase the error performance by combining SSK and pulse position modulation (PPM). It is shown that GSSK-II can achieve a linear spectral efficiency with respect to the number of transmit units, whereas all the other mentioned systems so far can only achieve a logarithmic spectral efficiency gain with increased number of TXs. However, the generalization of GSSK-II to any number of transmit units is not straightforward and the orthogonality of the signal set could only be provided for higher order modulations of PPM. Hence, the error performance of the system will decrease. The constellation design techniques for 2×2 and 3×3 MIMO-optical wireless communication (OWC) are given in [11] and [12], respectively. However,

¹This is the more generalized version of GSSK and will be referred to as GSSK-II throughout the paper. Note that the maximum spectral efficiency case for GSSK-II, when the duty cycle $\tau = 1$ [10], is considered in this paper.

This work was supported by EPSRC under Established Career Fellowship Grant EP/R007101/1. This work was also supported in part by the Scientific and Technical Research Council of Turkey (TUBITAK) under the 1003-Priority Areas R&D Projects support Program No. 218E034 and KAUST under Grant No. OSR-2016-CRG5-2958-02. A. Yesilkaya acknowledges the financial support from Zodiac Inflight Innovations (TriaGnoSys GmbH). A. A. Purwita acknowledges the financial support from Indonesian Endowment Fund for Education (LPDP). H. Haas acknowledges support from the Wolfson Foundation and the Royal Society.

the proposed technique requires a careful design procedure where an arbitrary number of light emitting diodes (LEDs) and constellation orders are not supported. Furthermore, the effect of user mobility on the system performance is not considered.

In this paper, a MIMO transmission method for OWC, referred to as flexible LED index modulation (FLIM), is proposed. In FLIM, the number of active TXs is not fixed, which greatly extends the transmission possibilities. Moreover, FLIM brings the flexibility to adjust power and/or error performance simply by choosing a proper transmission signal subset. In order to have a feasible detection complexity, a linear minimum mean squared error (MMSE) detector is used at the receiver. Lastly, a perturbed receiver ensures that the channel matrix of a mobile user is non-singular.

The rest of the paper is structured as follows: In Section II, the MIMO optical channel structure is described. The details of SM-based MIMO systems, including the proposed FLIM, is given in Section III. The average bit error probability (ABEP) performance of FLIM is compared with reference systems in Section IV. Conclusions are drawn in Section V.

Notation: Matrices and column vectors are written in bold uppercase and bold lowercase letters, respectively. The m^{th} row and n^{th} column element of a matrix \mathbf{A} is denoted by $A_{m,n}$. Similarly, the m^{th} element of a vector \mathbf{a} is given as a_m . The trace of a matrix, transpose of a matrix/vector and the Euclidean norm of a vector are expressed as $\text{tr}(\cdot)$, $(\cdot)^T$ and $\|\cdot\|$, respectively. A real normal distribution with mean μ and variance σ^2 is denoted by $\mathcal{N}(\mu, \sigma^2)$. The statistical expectation, argument maximum, argument minimum, flooring, dot product operators, Q-function, and the set of real numbers are given by $\mathbb{E}\{\cdot\}$, $\arg \max\{\cdot\}$, $\arg \min\{\cdot\}$, $\lfloor \cdot \rfloor$, \cdot , $Q(\cdot)$, and \mathbb{R} , respectively. Lastly, the $m \times m$ identity matrix and $n \times 1$ all-zeroes vector are denoted by \mathbf{I}_m and $\mathbf{0}_n$, respectively.

II. MIMO-OWC CHANNEL

In this work, we consider an optical MIMO application where each mobile user equipment (UE) is equipped with non-imaging receivers. In Fig. 1(a), the system structure is depicted where the luminaire is serving as the optical access point (AP) and the UE can be in any location within the attocell boundaries. Each optical AP and mobile UE is assumed to be equipped with N_t LEDs and N_r photo-diodes (PDs), respectively. As reported in [13], the line-of-sight (LoS) link is sufficient to accurately model a practical OWC system. Accordingly, the multipath signal contributions are negligible as long as the UE is not located at the corners of the room. The geometric parameters of the LEDs and PDs are given in vector notation where the origin is depicted in Fig. 1(a) as the point o . The unit normal vectors in x , y and z axes are given as \mathbf{n}_x , \mathbf{n}_y and \mathbf{n}_z , respectively. The locations of the i^{th} LED, j^{th} PD and UE are denoted by their position vectors as \mathbf{l}_i , \mathbf{p}_j and \mathbf{u} , respectively. Moreover, the unit normal vector of the i^{th} LED is given by \mathbf{n}_i . All the PDs are assumed to be placed on the same plane as depicted in Fig. 1(a). The relationship between \mathbf{u} and \mathbf{p}_j is given by $\mathbf{p}_j = \mathbf{u} + \bar{\mathbf{p}}_j$, where $\bar{\mathbf{p}}_j$ is the position vector of the j^{th}

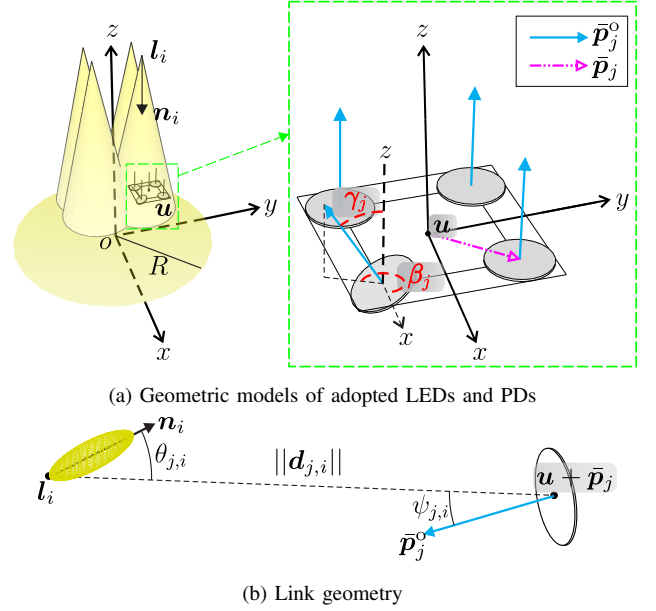


Fig. 1: Geometric details of the MIMO-OWC channel.

PD relative to the UE². The orientation of the j^{th} PD is defined by the unit orientation vector $\bar{\mathbf{p}}_j^o$. The polar angle of the j^{th} PD with respect to \mathbf{n}_z is defined by $\gamma_j = \mathbf{n}_z \cdot \bar{\mathbf{p}}_j^o$. Similarly, the azimuth angle of the j^{th} PD with respect to \mathbf{n}_x is given as $\beta_j = \mathbf{n}_x \cdot \tilde{\mathbf{p}}_j^o$ where $\tilde{\mathbf{p}}_j^o$ is the projection of the $\bar{\mathbf{p}}_j^o$ onto the xy -plane. Thus, the orientation vector could be expressed as $\bar{\mathbf{p}}_j^o = [\sin(\gamma_j) \cos(\beta_j), \sin(\gamma_j) \sin(\beta_j), \cos(\gamma_j)]$. It should be noted that all the LEDs in a luminaire are assumed to be facing downward ($-\mathbf{n}_z$ direction). Also, both the LEDs and PDs are assumed to be located at the corners of a square plane, which is the most common case in practical applications. Therefore, the LoS direct-current (DC) channel gain between the i^{th} LED and the j^{th} PD is given as follows [14], [15]:

$$H_{j,i} = \frac{(m+1)A_{\text{PD}}}{2\pi\|\mathbf{d}_{j,i}\|^{m+3}} (-\mathbf{n}_z \cdot \mathbf{d}_{j,i})^m (\bar{\mathbf{p}}_j^o \cdot \mathbf{d}_{j,i}) \mathbb{1}_{\kappa_{1/2}}(\psi_{j,i}), \quad (1)$$

where $i \in \{1, 2, \dots, N_t\}$ and $j \in \{1, 2, \dots, N_r\}$. The Lambertian mode number is defined as, $m = -1/\log_2(\Phi_{1/2})$ where $\Phi_{1/2}$ is the semi-angle of half power of the LED. The detector area of the PDs are denoted by A_{PD} . The angle of incidence between the i^{th} LED and the j^{th} PD, depicted in Fig. 1(b), is denoted as $\psi_{j,i}$. The Euclidean distance vector directed from the j^{th} PD to the i^{th} LED is given as, $\mathbf{d}_{j,i} = \mathbf{l}_i - \mathbf{p}_j = \mathbf{l}_i - \mathbf{u} - \bar{\mathbf{p}}_j$. The indicator function, $\mathbb{1}_{\kappa_{1/2}}(\cdot)$, defines the field-of-view (FoV) of PDs as follows:

$$\mathbb{1}_{\kappa_{1/2}}(x) = \begin{cases} 1, & \text{if } |x| \leq \kappa_{1/2} \\ 0, & \text{otherwise} \end{cases}$$

²The origin for the vectors with bar on top is the point \mathbf{u} .

where $\kappa_{1/2}$ is the half angle of the FoV of the PDs. Consequently, the optical channel matrix becomes

$$\mathbf{H} = \begin{bmatrix} H_{1,1} & \dots & H_{1,N_t} \\ \vdots & \ddots & \vdots \\ H_{N_r,1} & \dots & H_{N_r,N_t} \end{bmatrix}, \quad (2)$$

where $0 \leq H_{j,i} \leq 1$ and $H_{j,i} \in \mathbb{R}^+$, $\forall i, j$.

III. SYSTEM DESCRIPTION

The N_t -LED \times N_r -PD FLIM technique is detailed in this section. Accordingly, N_b -bits binary information vector $\mathbf{b}_u = [b_{u,0}, b_{u,1}, \dots, b_{u,N_b-1}]^T$ is generated by the user and fed into a mapping function $f_{\mathcal{M}}$. The *one-to-one* mapping rule encodes each \mathbf{b}_u onto a N_t -length transmission vector $\mathbf{s}_t = [s_{t,0}, s_{t,1}, \dots, s_{t,N_t-1}]^T$, where $\mathbf{b}_u \in \mathbb{B}$, $\mathbf{s}_t \in \mathbb{S}$ for $1 \leq u, t \leq C$. The binary permutation vector set and transmit vector set are denoted by \mathbb{B} and \mathbb{S} , respectively. The cardinality of the sets are determined by the chosen modulation technique as $|\mathbb{B}| = |\mathbb{S}| = C$. It should be noted that $C = 2^n$ where $n \in \mathbb{Z}$. In some modulations such as GSM, GSM-II, GSSK and FLIM, the total number of symbols, K , is not a power of two. Hence, a subset of the transmit symbols must be chosen such that $C = 2^{\lfloor \log_2(K) \rfloor}$. The number of bits per transmit symbol becomes $N_b = \log_2(C)$. The mapping function $f_{\mathcal{M}}$ is given by $f_{\mathcal{M}} : \mathbf{b}_u \in \mathbb{B} \rightarrow \mathbf{s}_t \in \mathbb{S}$, where $b_{u,i} \in \{0, 1\}$ and $s_{t,j} \in \mathcal{M}$ for $0 \leq i \leq N_b - 1$, $0 \leq j \leq N_t - 1$. It is important to note that \mathbf{s}_t conveys both the constellation and spatial symbols also, \mathcal{M} denotes the finite modulation alphabet. As the intensity modulation and direct detection (IM/DD) signals are constrained to be real and positive valued, the forward driving current of the LEDs, I_f , is assumed to be modulated by unipolar M -ary pulse amplitude modulation (PAM). Thus, the unipolar M -PAM alphabet is given by

$$\mathcal{M} = \left\{ I_f \in \mathbb{R}^+ : I_L + \frac{I_U - I_L}{M-1} k, \quad k \in \{0, 1, \dots, M-1\} \right\}, \quad (3)$$

where M is the PAM order. The upper and lower limits of the forward driving current are given by I_U and I_L , respectively. It is reported in [16] that the error performance of PAM is highly dependent on the non-linear characteristics of the LEDs. Therefore, it is important to choose I_U and I_L within the dynamic range of an LED. In SM-based systems, I_f could be zero which corresponds to the *inactive* state of an LED. The locations of the *inactive* LEDs and values of the *active* LEDs are the unique signature of the adopted modulation technique. Thus, the transmission vector set for SM is given for $N_t = 3$ as follows:

$$\mathbb{S}^{\text{SM}} = \left\{ \begin{bmatrix} m_0 \\ 0 \\ 0 \end{bmatrix}, \begin{bmatrix} 0 \\ m_1 \\ 0 \end{bmatrix}, \begin{bmatrix} 0 \\ 0 \\ m_2 \end{bmatrix} \right\}.$$

The transmitted constellation symbols are given by $m_i \in \mathcal{M}$, $\forall i$. Note that the $N_t = 3$ is only chosen for the presentation simplicity, refer to Fig. 2, in practice N_t is power of two to achieve the adequate bit labelling. Similar to SM, the

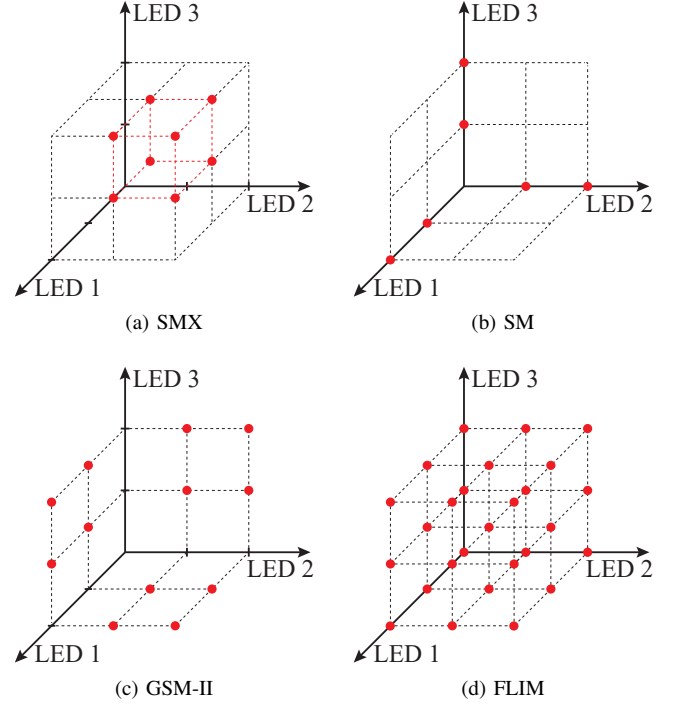


Fig. 2: Transmission symbol possibilities are depicted for (a) SMX, (b) SM, (c) GSM-II and (d) FLIM. The red dots are depicting the possible PAM symbols could be transmitted from the LEDs when $M = 2$ and $N_t = 3$.

transmission vector sets for GSM-II and spatial multiplexing (SMX) are given by

$$\mathbb{S}^{\text{GSM-II}}(2) = \left\{ \begin{bmatrix} m_0 \\ m_1 \\ 0 \end{bmatrix}, \begin{bmatrix} m_2 \\ 0 \\ m_3 \end{bmatrix}, \begin{bmatrix} 0 \\ m_4 \\ m_5 \end{bmatrix} \right\} \quad \text{and} \quad \mathbb{S}^{\text{SMX}} = \begin{bmatrix} m_0 \\ m_1 \\ m_2 \end{bmatrix},$$

where the GSM-II transmit vector for N_a active transmitters is denoted as $\mathbb{S}^{\text{GSM-II}}(N_a)$. It should be noted that both SM and SMX are the special cases of GSM-II with $\mathbb{S}^{\text{SM}} = \mathbb{S}^{\text{GSM-II}}(1)$ and $\mathbb{S}^{\text{SMX}} = \mathbb{S}^{\text{GSM-II}}(N_t)$. In FLIM, the constraint of a predetermined number of active LEDs is relaxed, $N_a \in \{0, 1, 2, \dots, N_t\}$, which extends the transmission alphabet significantly. Thus, the transmission vector set for FLIM becomes

$$\mathbb{S}^{\text{FLIM}} = \{\mathbf{0}_{N_t}, \mathbb{S}^{\text{SM}}, \mathbb{E}^{\text{GSM-II}}, \mathbb{S}^{\text{SMX}}\}, \quad (4)$$

where the universal set for the activation patterns of GSM-II is given by:

$$\mathbb{E}^{\text{GSM-II}} = \bigcup_{N_a=2}^{N_t-1} \mathbb{S}^{\text{GSM-II}}(N_a). \quad (5)$$

It should be noted that all-off, $\mathbf{0}_{N_t}$, and the all-on, \mathbb{S}^{SMX} , patterns are strictly avoided in radio frequency (RF) based SM systems [17], [18]. However, the information carrying signal can be zero or near zero in OWC due to the LED turn-on current. The all-on pattern is also utilized in FLIM in order to enlarge the transmit vector set. The larger transmission vector set brings the advantage of flexibility to FLIM by choosing a subset to optimize: either error performance or power efficiency. The transmit symbol spaces for the aforementioned SM-based

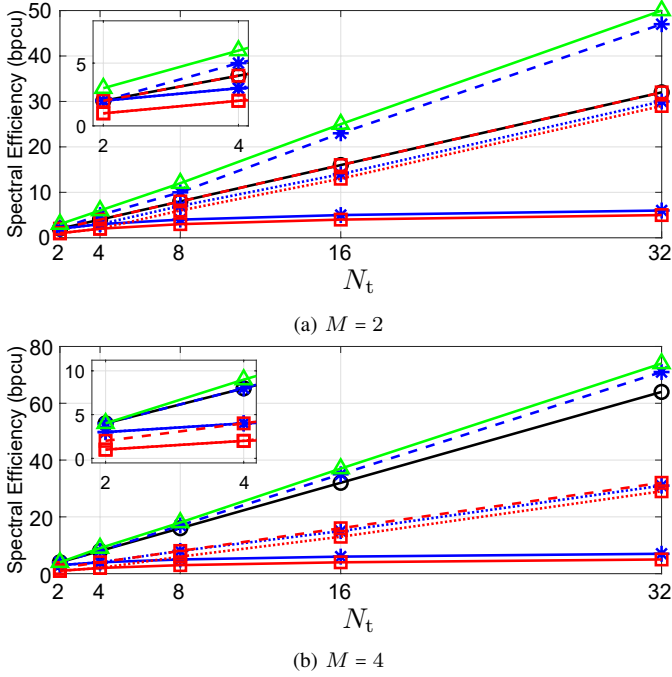


Fig. 3: Spectral efficiency comparison for SSK (—■—), GSSK (·····■·····), GSSK-II (—■—), SM (—*—), GSM (·····*·····), GSM-II (—*—), SMX (—●—) and FLIM (—▲—).

systems including FLIM is depicted for the cases where $N_t = 3$ and $M = 2$ in Fig. 2. It can be seen from the figure that FLIM contains the symbols of all the other systems along with its unique symbols. Therefore, the spectral efficiency of FLIM becomes

$$\eta_{\text{FLIM}} = \lfloor N_t \log_2(M+1) \rfloor \text{ bits per channel use (bpcu)}. \quad (6)$$

The factor $(M+1)$ in (6) emerges from the relaxed number of LEDs, by using the binomial theorem, which yields an enlarged transmit set. However, this advantage will diminish while M increases. Note from (6) also that the relaxation of the number of active LEDs is essentially equivalent to extending the M -ary PAM into $(M+1)$ -ary constellation, $\tilde{\mathcal{M}} = \{I_0\} \cup \mathcal{M}$. The *zero* symbol is given by $I_0 \in [0, I_L]$. Therefore, unlike conventional systems, odd numbered M values could be utilized in FLIM. The spectral efficiency comparisons between FLIM and the reference systems are provided in Fig. 3 where it can be seen that the spectral efficiency advantage of FLIM is still effective when $M = 2$ and $M = 4$. In practice, the PAM modulation order is chosen to be within $2 \leq M \leq 8$ in order to achieve a feasible error performance.

Then, the transmit signal vector \mathbf{s}_t is fed to the digital-to-analog conversion (DAC) and electrical-to-optical conversion (E/O) before the transmission. The optical domain transmit vector passes through an $N_t \times N_r$ optical channel matrix \mathbf{H} . At the RX side, the electrical domain received signal is obtained after the optical-to-electrical conversion (O/E) and analog-to-digital conversion (ADC). The baseband received signal vector $\mathbf{y} = [y_0, y_1, \dots, y_{N_r}]^T \in \mathbb{R}_{N_r \times 1}$ is given by $\mathbf{y} = \mathbf{r}_t + \mathbf{n}$, where $N_r \times 1$ optical received signal vector is given by $\mathbf{r}_t = \mathbf{H}\mathbf{s}_t =$

$[r_{t,0}, r_{t,1}, \dots, r_{t,N_r-1}]^T$. The $N_r \times 1$ additive white Gaussian noise (AWGN) vector is denoted by $\mathbf{n} \in \mathbb{R}_{N_r \times 1}$. The elements of \mathbf{n} follow $\mathcal{N}(0, \sigma_n^2)$. In this paper, without loss of generality, the values of E/O, O/E, ADC and DAC coefficients are assumed to be one. Thus, the received electrical power expression is given as follows:

$$P_{\text{elec}} = \sum_{i=1}^{N_r} \mathbb{E}\{r_{t,i}^2\} = \sum_{i=1}^{N_r} \sum_{j=1}^{N_t} H_{i,j}^2 \mathbb{E}\{s_{t,j}^2\} + \sum_{i=1}^{N_r} \sum_{k=1}^{N_t} \sum_{l=1, l \neq k}^{N_t} H_{i,k} H_{i,l} \mathbb{E}\{s_{t,k}\} \mathbb{E}\{s_{t,l}\}. \quad (7)$$

The probability mass function (PMF) for i^{th} element of \mathbf{s}_t is given by:

$$p_{s_{t,i}}(x) = \frac{1 - \nu_i}{M} + \nu_i \delta[x], \quad (8)$$

where ν_i denotes the probability of a *zero* occurring in $s_{t,i}$. It should be noted that the parameter ν_i changes depending on the adopted transmission technique. In SMX, $\nu_i = 0, \forall i$, whereas it is $\nu_i = 1/N_t, \forall i$ in the conventional SM. For GSM-II and FLIM, the values of the ν_i 's are a parameter of the chosen transmission subset. The electrical power of the $s_{t,i}$ in (7) is calculated by using (8) as

$$\mathbb{E}\{s_{t,i}^2\} = (1 - \nu_i) \left(I_L^2 + I_L(I_U - I_L) + \frac{2M-1}{6(M-1)}(I_U - I_L)^2 \right). \quad (9)$$

Hence, the received electrical signal-to-noise-ratio (SNR) per bit becomes

$$\frac{E_{b,\text{elec}}}{N_0} = \frac{P_{\text{elec}}}{\eta N_0}. \quad (10)$$

The parameter N_0 denotes the single sided noise power spectral density, $\sigma_n^2 = N_0 B$ where B is the bandwidth of the effective noise process. In this paper, B is assumed to be one without loss of generality. The spectral efficiency of the adopted modulation technique in terms of average bits per symbol is denoted by η .

Next, the maximum-likelihood (ML) detector jointly estimates both the spatial and constellation symbols by using the received vector \mathbf{y} as follows:

$$\hat{\mathbf{s}}_t = \arg \max_{\mathbf{s}_t \in \mathcal{S}} p(\mathbf{y} | \mathbf{H}\mathbf{s}_t) = \arg \min_{\mathbf{s}_t \in \mathcal{S}} \|\mathbf{y} - \mathbf{H}\mathbf{s}_t\|. \quad (11)$$

The feed-forward equalization block of the ML detector is given by $\mathbf{F} = \mathbf{I}_{N_r}$. Lastly, the transmitted information bits are recovered by an inverse one-to-one mapping, $f_{\mathcal{M}}^{-1}$ as $\hat{\mathbf{b}}_i = f_{\mathcal{M}}^{-1}(\hat{\mathbf{s}}_i)$. The bit error probability (BEP) for the optimal ML detector is not straightforward to obtain due to the joint error probabilities of the transmission symbols. However, the BEP could be upper bounded by the union bound as follows:

$$P_b \leq \frac{1}{C \log_2(C)} \sum_{i=1}^C \sum_{j=1}^C d_H(\mathbf{s}_i, \mathbf{s}_j) P(\mathbf{s}_i \rightarrow \mathbf{s}_j) \quad (12)$$

where the Hamming distance between the binary labels of s_i and s_j is denoted by $d_H(s_i, s_j)$. The pairwise error probability (PEP) between s_i and s_j is given by

$$P(s_i \rightarrow s_j) = Q\left(\frac{\|\mathbf{H}(s_i - s_j)\|}{2\sigma_n}\right). \quad (13)$$

It is worth noting from (11) that the ML detector is optimal in terms of error probability as s_t 's are equally likely. However, the size of the search space and the receiver complexity are proportional to the cardinality of the chosen set. It can be inferred from $|\mathcal{S}^{\text{SMX}}|$, $|\mathcal{S}^{\text{GSM-II}}|$ and $|\mathcal{S}^{\text{FLIM}}|$ that the search space is an exponential function of N_t . Therefore, in this paper, we are investigating an MMSE based MIMO detector which has a linear complexity with respect to N_t .

A. Low Complexity MMSE Detector

Unlike the optimal ML detector, which determines both spatial and constellation symbols jointly, the linear MMSE detector treats the elements of the transmission vector individually. Firstly, the coupling effect of the parallel MIMO channel is reversed by a feed-forward MMSE filter \mathbf{F} as

$$\mathbf{F} = \mathbf{R}_s \mathbf{H}^T (\mathbf{H} \mathbf{R}_s \mathbf{H}^T + \mathbf{R}_w)^{-1}, \quad (14)$$

where $\mathbf{R}_s \triangleq E\{\mathbf{s}_t \mathbf{s}_t^T\}$ is the autocorrelation matrix averaged over all the possibilities of s_t . The autocorrelation matrix of the coloured noise after filtering, $\hat{\mathbf{y}} = \mathbf{F} \mathbf{y}$, is given by $\mathbf{R}_w = E\{\mathbf{w} \mathbf{w}^T\} = \sigma_w^2 \mathbf{I}_{N_r}$. Secondly, the transmitted symbols are detected by an element-wise detector as follows:

$$\hat{s}_i = \arg \max_{\substack{0 \leq k \leq M \\ s_k \in \mathcal{M}}} p(\hat{y}_i | s_k) = \arg \min_{\substack{0 \leq k \leq M \\ s_k \in \mathcal{M}}} |\hat{y}_i - s_k|. \quad (15)$$

It should be noted from (15) that the number of active LEDs is relaxed in FLIM as given by (4). Thus, the RX has no information about the number of active LEDs in the transmitted symbols, whereas this is not the case in SMX and SM-based systems. Therefore, I_0 can be considered as one of the constellation symbols in FLIM as mentioned previously. By using (3), the M -ary PAM constellation set is extended to $\bar{\mathcal{M}} = \{0\} \cup \mathcal{M}$ for $k \in \{0, 1, \dots, M\}$. The singleton $\{0\}$ corresponds to the $(M+1)^{\text{th}}$ element of the $\bar{\mathcal{M}}$.

IV. COMPUTER SIMULATIONS

In this section, computer simulation results for 4×4 systems are presented to first investigate the effect of an angle diversity receiver (ADR) on the condition number (CN) distribution. Then, the BEP performance comparisons between FLIM, GSM-II and SMX when they employ ADR are obtained by the use of Monte Carlo simulations. The optical attocell structure considered in the simulations is depicted in Fig. 1(a). The location of the mobile UE within the attocell is defined by polar coordinates, $(R_{\text{UE}}, \omega_{\text{UE}})$. The radius and polar angle parameters are denoted by R_{UE} and ω_{UE} , respectively where $0 \leq R_{\text{UE}} \leq R_{\text{cell}}$ and $0 \leq \omega_{\text{UE}} \leq 2\pi$. The cell radius, as depicted in Fig. 1, is defined as the region where the maximum optical power received from an LED is halved. Thus, $R_{\text{cell}} = \rho_{\text{cell}} (H_{\text{lum}} - H_{\text{UE}})$ where $\rho_{\text{cell}} = \sqrt{4^{1/(m+3)} - 1}$. The

TABLE I: Simulation Parameters

Parameter	Description	Value
R_{cell}	Radius of the optical attocell.	100 cm
L	Separation between two LEDs.	2 cm
H_{lum}	Height of the luminaire (optical AP).	300 cm
H_{human}	Average height of the human.	180 cm
H_{UE}	Average height of the mobile device.	144 cm
A_{PD}	Area of the PD.	1 cm ²
$\Phi_{1/2}$	Semi-angle of half power of the LED.	60°
$\kappa_{1/2}$	FoV of the PD.	85°
ω_{UE}	Polar angle of the mobile user location.	[0 2 π] rad
R_{UE}	Radius of the mobile user location.	[0 100] cm
I_{U}	The upper limit for the I_f .	800 mA [20]
I_{L}	The lower limit for the I_f .	500 mA [20]

parameters, H_{lum} and H_{UE} , denote the height of the luminaire and the distance of the UE from the floor, respectively. Their values are adopted from [19]. Moreover, the LEDs are chosen as Lambertian transmitters with $\Phi_{1/2} = 60^\circ$. Similarly, PDs are assumed to have a FoV of 85° . The entire set of simulation parameters and their values are given in Table I.

In this work, two PD configurations of the receivers; square and square-perturbed, which are depicted in Fig. 4(a) and Fig. 4(b), respectively are considered. Accordingly, in the square receiver, each LED is aligned with a PD where the separation between the PDs is 2 cm. In the perturbed square receiver, the PD formation stays the same however, random polar and azimuth angles are introduced to each PD in order to break the potential rank deficiency. The polar and azimuth angles of the perturbed receiver are taken as $\{\{\gamma_j, \beta_j\}_1^{N_r}\} = \{\{-5, 6\}, \{-8, 1\}, \{-10, 2\}, \{15, 1\}\}$ degrees. It is worth noting that any arbitrary selection of the polar and azimuth angles will break the symmetry in the channel matrix. A deeper investigation on the tilt angles and their optimal values will be carried out in future work.

The performance of the suboptimal MMSE detector is closely related to the CN, as stated in the previous section. Therefore, the channel matrix CN distributions for a mobile UE with the adopted PD structures is depicted in Fig. 5, by using polar plots. The values of the CN are given for any location of the mobile UE within an attocell. The resolution of the R_{UE} and ω_{UE} are taken as 2.5 centimetres and 1 degree, respectively. The CN distribution of the square receiver is given in Fig. 5(a). As can be seen from the figure, the CN of the square receiver is approximately 8 dB smaller in the cell centre compared to the cell edges. It can be inferred from (1) that the MIMO channel matrix elements get smaller at the cell edges due to the inverse square distance law. Thus, the linear dependency between the rows and/or columns increases, which effectively yields a high CN. The average CN achieved by the square receiver becomes 62.14 dB with a standard deviation of 1.89 dB.

In Fig. 5(b), the CN distribution of the square-perturbed receiver is depicted for the same scale. As seen from the

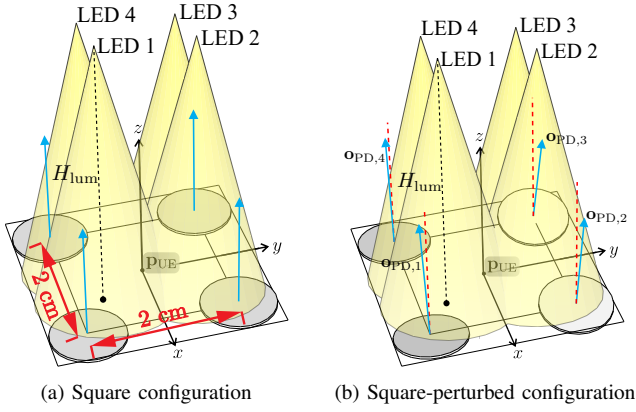


Fig. 4: Structure of the (a) typical receiver (a) and (b) ADR.

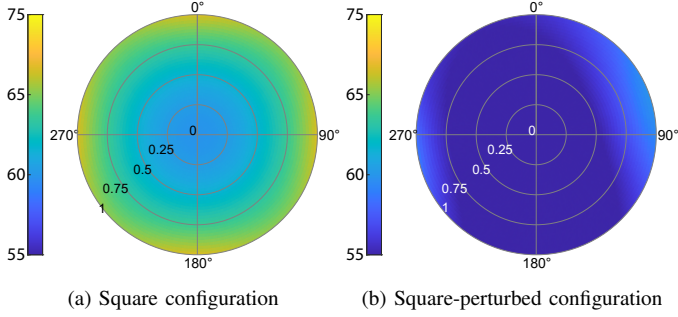


Fig. 5: CN distribution plots (in dB) for adopted receiver configurations.

figure, the CN is dramatically reduced as the MIMO channel elements are differentiated with the aid of random perturbation. Moreover, the distribution of the CN is almost flat, except for some small areas near the cell edges. Again, due to the inverse square law and random direction of the PDs, relatively high CN regions are observed in the north-east and south-west edges of the polar plot. The square-perturbed receiver structure achieves an average CN of 54.11 dB with the standard deviation of 1.52 dB. Hence, the random perturbation of the PDs reduces the average CN and standard deviation by around 8 and 0.37 dB, respectively. Consequently, in ABEP simulations, both proposed FLIM and the reference systems are assumed to be utilizing the square-perturbed structure at the receiving UE.

In Fig. 6, the ABEP comparisons for the FLIM, GSM-II and SMX are given with respect to the transmit electrical SNR per bit. Accordingly, all three systems employ low-complexity linear MMSE for symbol detection and a square-perturbed PD structure for enhanced detector performance. The plots are given for two spectral efficiency values; low ($\eta = 4$ bpcu), in Figs. 6(a), (b), and medium/high ($\eta = 8$ bpcu), in Figs. 6(c), (d). Furthermore, the impact of the CN on the ABEP performance is investigated for cell centre ($R_{UE} = 0$, $\omega_{UE} = 0^\circ$) and edge ($R_{UE} = 1$, $\omega_{UE} = 90^\circ$) locations of the UE, depicted in Figs. 6(a), (c) and Figs. 6(b), (d), respectively. It is important to note that the ABEP curves are obtained by running Monte-Carlo simulations for 10^7 transmit symbol realizations. In order to fairly compare the BEPs of multiple systems under different channel conditions,

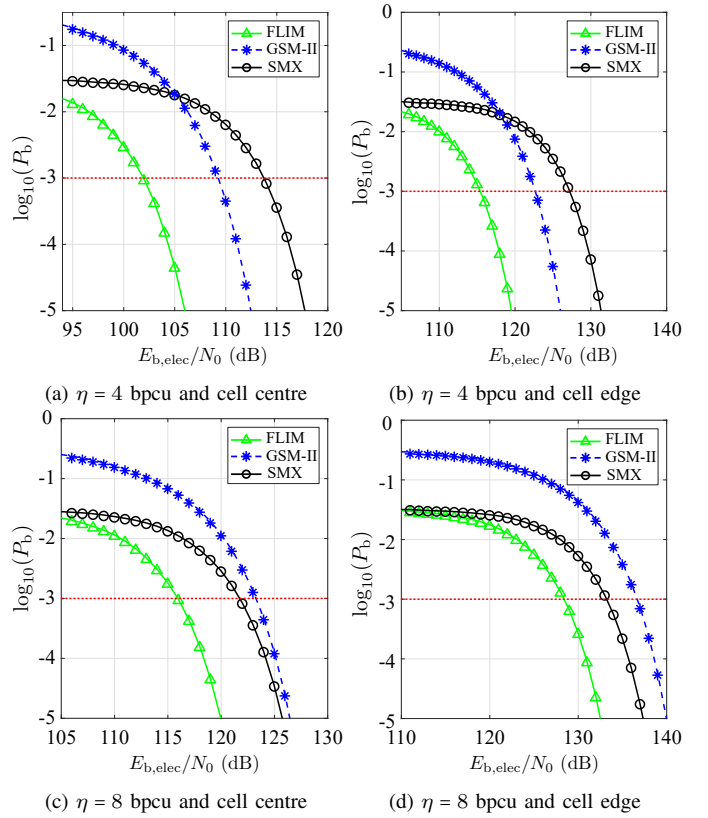


Fig. 6: ABEP vs. transmit $E_{b,elec}/N_0$ comparison for GSM-II, SMX and FLIM systems at: (a) ($R_{UE} = 0$, $\omega_{UE} = 0^\circ$) and $\eta = 4$ bpcu, (b) ($R_{UE} = 1$, $\omega_{UE} = 90^\circ$) and $\eta = 4$ bpcu, (c) ($R_{UE} = 0$, $\omega_{UE} = 0^\circ$) and $\eta = 8$ bpcu and (d) ($R_{UE} = 1$, $\omega_{UE} = 90^\circ$) and $\eta = 8$ bpcu.

the transmit electrical SNR expression obtained by (9) must be used. Since the magnitude of the elements in the optical MIMO channel is in the order of 10^{-4} and 10^{-5} for the cell centre and edges, respectively, the electrical path loss at the receiver becomes -80 and -100 dB. Both FLIM and GSM-II techniques have some degree of flexibility in the transmission signal set design. Thus, in our simulations, a suboptimal signal set design and bit labelling algorithm is adopted for FLIM in order to reduce the system complexity. Accordingly, the suboptimal design matches the minimum Euclidean distance elements with the largest Hamming distances. Whereas GSM-II takes the advantage of optimal signal set design and bit labelling which is subject to minimize (12). Since the entire transmission symbols set is used in SMX, only the Gray bit labelling is adopted. Lastly, the number of active LEDs are fixed to the number $N_a = N_t/2$ in GSM-II as this yields the maximum spectral efficiency.

In Figs. 6(a) and (b), the ABEP vs. transmit $E_{b,elec}/N_0$ performance of FLIM is compared with GSM-II and SMX for $\eta = 4$ bpcu when the mobile UE is located at the cell centre and edge, respectively. As can be seen from both figures, FLIM outperforms GSM-II and SMX approximately 7 and 11 dB, respectively in the high SNR regime. The performance gain in FLIM, compared to the reference systems, comes from the smaller modulation order requirement to achieve the

target bit rate. Accordingly, the M values in order to achieve $\eta = 4$ bpcu with FLIM, GSM-II and SMX systems become, $M_{\text{SMX}} = 2$, $M_{\text{GSM-II}} = 2$ and $M_{\text{FLIM}} = 1$. Unlike GSM-II and SMX, FLIM is able to retain high multiplexing gains without sacrificing the energy efficiency benefits of the LED index domain utilization. The location of the mobile UE and related channel matrix coefficients are other important factors for the system performance. The difference between the curves when the UE is located at the cell centre and edge is around 13 dB in the high SNR regime for $\eta = 4$ bpcu. The reason for this is two-fold; the difference in (i) CN and (ii) element-wise magnitudes of the MIMO channel matrices. Specifically, CNs at the cell centre and edge are 52.76 and 59.41 dB, respectively. Furthermore, the magnitudes of the channel matrix elements are approximately 10 times larger at the cell centre compared to the edge.

In Figs. 6(c) and (d), the plots are given for $\eta = 8$ bpcu, where $M_{\text{SMX}} = 4$, $M_{\text{GSM-II}} = 8$ and $M_{\text{FLIM}} = 3$. Similarly, FLIM outperforms GSM-II and SMX by approximately 7 and 6 dB in Fig. 6(c) and 8 and 4 dB in Fig. 6(d), respectively. Again, FLIM takes advantage of its extended transmission symbols set with a smaller modulation order. It is important to note that the SMX outperforms GSM-II both in the cell centre and the edge for $\eta = 8$ bpcu. This can also be explained by the higher modulation size requirement of the GSM-II to achieve the target bit rate. In parallel, with the low spectral efficiency application, the difference between all the systems when the UE is located at the cell centre and edge also becomes 13 dB in the high SNR regime. Lastly, the curves for the FLIM, GSM-II and SMX at the cell centre are shifted to the right-hand side by 14, 14 and 8 dB, respectively when the target bit rate is doubled. For the cell edge, the values become 13, 14 and 6 dB, respectively. This is due to the reduced minimum Euclidean distance in the transmission symbols set that is imposed by the increase in M .

V. CONCLUSIONS

In this paper, a transmission technique for MIMO-OWC, introduced as FLIM, has been presented. Unlike conventional systems, the proposed method takes advantage of the relaxed number of active LEDs per time instance. Thus, the transmission symbol set is greatly extended in FLIM. The additional symbols can be used to enhance the error performance and/or power efficiency by subset selection. Moreover, a perturbed receiver structure has also been proposed in order to cope with the rank deficiency which paves the way for low-complexity MMSE detection. Computer simulations results have shown that FLIM achieves a better error performance compared to GSM-II and SMX. Consequently, the enhanced multiplexing gain and power efficiency makes FLIM a highly suitable candidate for next generation MIMO-OWC applications. The complexity/time analysis of the proposed technique and the optimal tilt angle derivations are reserved for future work.

REFERENCES

- [1] R. Mesleh, H. Haas, C. W. Ahn, and S. Yun, "Spatial modulation - a new low complexity spectral efficiency enhancing technique," in *Proc. 1st Int. Conf. Commun. Netw. in China*, Beijing, China, Oct 2006, pp. 1–5.
- [2] Y. A. Chau and S.-H. Yu, "Space modulation on wireless fading channels," in *Proc. IEEE 54th Veh. Technol. Conf. (VTC Fall)*, vol. 3, Atlantic City, NJ, USA, Oct 2001, pp. 1668–1671 vol.3.
- [3] J. Jeganathan, A. Ghrayeb, L. Szczecinski, and A. Ceron, "Space shift keying modulation for MIMO channels," *IEEE Trans. Wireless Commun.*, vol. 8, no. 7, pp. 3692–3703, Jul. 2009.
- [4] J. Jeganathan, A. Ghrayeb, and L. Szczecinski, "Generalized space shift keying modulation for MIMO channels," in *Proc. IEEE 19th Int. Symp. Pers. Indoor Mobile Radio Commun.*, Cannes, France, Sept 2008, pp. 1–5.
- [5] A. Younis, N. Serafimovski, R. Mesleh, and H. Haas, "Generalised spatial modulation," in *Proc. 44th Asilomar Conf. Signals, Syst. Comput.*, Pacific Grove, CA, USA, Nov 2010, pp. 1498–1502.
- [6] J. Fu, C. Hou, W. Xiang, L. Yan, and Y. Hou, "Generalised spatial modulation with multiple active transmit antennas," in *Proc. IEEE GLOBECOM Workshops*, Miami, FL, USA, Dec 2010, pp. 839–844.
- [7] J. Wang, S. Jia, and J. Song, "Generalised spatial modulation system with multiple active transmit antennas and low complexity detection scheme," *IEEE Trans. Wireless Commun.*, vol. 11, no. 4, pp. 1605–1615, Apr. 2012.
- [8] K. Ntontin, M. D. Renzo, A. Perez-Neira, and C. Verikoukis, "Performance analysis of multistream spatial modulation with maximum-likelihood detection," in *Proc. IEEE Global Commun. Conf. (GLOBECOM)*, Atlanta, GA, USA, Dec 2013, pp. 1590–1594.
- [9] W. O. Popoola, E. Poves, and H. Haas, "Error performance of generalised space shift keying for indoor visible light communications," *IEEE Trans. Commun.*, vol. 61, no. 5, pp. 1968–1976, May 2013.
- [10] W. Popoola, E. Poves, and H. Haas, "Generalised space shift keying for visible light communications," in *Proc. 8th Int. Symp. Commun. Syst., Netw. Digit. Signal Process. (CSNDSP)*, Poznan, Poland, Jul. 2012, pp. 1–4.
- [11] K. Xu, H. Yu, Y. Zhu, and H. Cai, "Channel-adaptive space-collaborative constellation design for MIMO VLC with fast maximum likelihood detection," *IEEE Access*, vol. 5, pp. 842–852, 2017.
- [12] Y.-J. Zhu, W.-F. Liang, C. Wang, and W.-Y. Wang, "Energy-efficient constellations design and fast decoding for space-collaborative MIMO visible light communications," *Optics Commun.*, vol. 383, pp. 260 – 273, 2017.
- [13] C. Chen, D. A. Basnayaka, and H. Haas, "Downlink performance of optical attocell networks," *J. Lightw. Technol.*, vol. 34, no. 1, pp. 137–156, Jan. 2016.
- [14] J. M. Kahn and J. R. Barry, "Wireless infrared communications," *Proc. IEEE*, vol. 85, no. 2, pp. 265–298, Feb 1997.
- [15] A. Yesilkaya, R. Bian, I. Tavakkolnia, and H. Haas, "OFDM-based optical spatial modulation," *IEEE J. Sel. Topics Signal Process.*, vol. 13, no. 6, pp. 1433–1444, 2019.
- [16] H. Qian, S. Cai, S. Yao, T. Zhou, Y. Yang, and X. Wang, "On the benefit of DMT modulation in nonlinear VLC systems," *Opt. Express*, vol. 23, no. 3, pp. 2618–2632, Feb 2015.
- [17] M. D. Renzo and H. Haas, "On transmit diversity for spatial modulation MIMO: Impact of spatial constellation diagram and shaping filters at the transmitter," *IEEE Trans. Veh. Technol.*, vol. 62, no. 6, pp. 2507–2531, Jul. 2013.
- [18] P. Liu, M. D. Renzo, and A. Springer, "Variable- N_u generalized spatial modulation for indoor LOS mmWave communication: Performance optimization and novel switching structure," *IEEE Trans. Commun.*, vol. 65, no. 6, pp. 2625–2640, Jun. 2017.
- [19] A. Yesilkaya, T. Cogalan, E. Panayirci, H. Haas, and H. V. Poor, "Achieving minimum error in MISO optical spatial modulation," in *Proc. IEEE Int. Conf. Commun. (ICC)*, Kansas City, MO, USA, May 2018, pp. 1–6.
- [20] "CREE XLamp XM-L EasyWhite LEDs. [Online]," https://www.cree.com/led-components/media/documents/XLampXML_EZW.pdf, accessed: 31-08-2020.